

A New Microlensing Event in the Doubly-Imaged Quasar Q 0957+561

Laura J. Hainline¹, Christopher W. Morgan¹, Joseph N. Beach¹, C. S. Kochanek², Hugh C. Harris³, Trudy Tilleman³, Ross Fadely⁴, Emilio E. Falco⁵, and Truong X. Le¹

ABSTRACT

We present evidence for ultraviolet/optical microlensing in the gravitationally lensed quasar Q 0957+561. We combine new measurements from our optical monitoring campaign at the United States Naval Observatory, Flagstaff (USNO) with measurements from the literature and find that the time-delay-corrected r band flux ratio $m_A - m_B$ has increased by ~ 0.1 magnitudes over a period of five years beginning in the fall of 2005. We apply our Monte Carlo microlensing analysis procedure to the composite light curves, obtaining a measurement of the optical accretion disk size, $\log\{(r_s/\text{cm})[\cos(i)/0.5]^{1/2}\} = 16.2 \pm 0.5$, that is consistent with the quasar accretion disk size – black hole mass relation.

Subject headings: gravitational lensing: strong — gravitational lensing: micro — accretion disks — quasars: individual (Q 0957+561)

1. INTRODUCTION

The history of microlensing in the $z_s = 1.405$ quasar Q 0957+561 (hereafter Q0957), the first confirmed gravitational lens system, is paradoxically simple yet complex. The

¹Department of Physics, United States Naval Academy, 572C Holloway Rd, Annapolis, MD 21402, USA; hainline@usna.edu, cmorgan@usna.edu, m110480@usna.edu, m113678@usna.edu

²Department of Astronomy, The Ohio State University, 140 West 18th Ave, Columbus, OH 43210, USA; ckochanek@astronomy.ohio-state.edu

³United States Naval Observatory, Flagstaff Station, 10391 West Naval Observatory Road, Flagstaff, AZ 86001-8521, USA; hch@nobs.navy.mil, trudy@nobs.navy.mil

⁴Department of Astronomy, Haverford College, 370 Lancaster Avenue, Haverford, PA 19041, USA; rfadely@haverford.edu

⁵Harvard-Smithsonian Center for Astrophysics, 60 Garden St, Cambridge, MA 02138, USA; falco@cfa.harvard.edu

possibility of microlensing in this double-image, wide-separation ($\sim 6''$) quasar was proposed by Chang & Refsdal (1979) soon after its discovery by Walsh, Carswell, & Weymann (1979). Controversy over the time delay, currently accepted to be $\Delta t_{AB} = 417$ days (e.g., Vanderriest et al. 1989; Schild 1990; Kundić et al. 1997; Shalyapin et al. 2008), spawned numerous time variability studies of Q0957 at optical and radio wavelengths which produced a wealth of monitoring data. Microlensing of the quasar on long time scales was soon established by a change in the time delay-corrected magnitude difference of the two images of $\Delta(m_A - m_B) \sim 0.25$ over the course of five years, observed by Vanderriest et al. (1989) and confirmed by Pelt et al. (1998). However, after that initial event, occurring between 1982–1986, the difference light curve (the difference between the light curve for image A and the time-delay shifted light curve for image B) became nearly constant. Debate over the existence of measurable variability in the flux ratio percolated through the literature, with some authors reporting variability in the flux ratio on the order of several hundredths of a magnitude over timescales of weeks, days, and hours, while other groups simultaneously concluded that no microlensing with amplitude $|\Delta(m_A - m_B)| \gtrsim 0.05$ was detected (see, e.g., Gil-Merino et al. 2001; Schmidt & Wambsganss 2010, for summaries and references). As the dispute surrounding the existence of short-timescale microlensing evolved, the absence of long-time scale microlensing became increasingly evident from the difference light curve’s steadiness over roughly 20 years. The only report of a possible long-time scale event after 1986, that of Ovaldsen et al. (2003) of 5%-level variability over 300 days, was not corroborated independently by Wambsganss et al. (2000) with data taken over the same time period. Studies as recent as Shalyapin et al. (2008) find no evidence for microlensing in their data.

With the development of numerical simulation methods to analyze microlensing observations (e.g., Kochanek 2004; Bate, Webster, & Wyithe 2007; Blackburne et al. 2011), quasar microlensing has meanwhile become a powerful tool with which to quantitatively study the properties of lens galaxies and the structure of quasars. Although quasars and individual stars in lens galaxies cannot be resolved by conventional telescopes, by modeling the amplitudes of microlensing fluctuations we can measure the size of the continuum emission region, the masses and velocities of the stellar microlenses, and the stellar-to-dark mass fraction in the lens galaxy (e.g., Kochanek 2004; Pooley et al. 2007; Morgan et al. 2008; Mediavilla et al. 2009; Dai et al. 2010). Through analysis of microlensing variability at multiple wavelengths, the surface brightness profile of the quasar may be measured (e.g., Poindexter et al. 2008; Eigenbrod et al. 2008). We are now moving into an era in which theoretical models of accretion disk structure can be tested with significant samples of lensed quasars, resulting in the observational confirmation of a relation between central black hole mass and accretion disk size (Morgan et al. 2010), as well as the temperature profile of the Shakura & Sunyaev (1973)

thin accretion disk model (e.g., Poindexter et al. 2008; Anguita et al. 2008; Mosquera et al. 2011).

Since the central black hole in Q0957 lies at the high end of the quasar black hole mass function ($1.0 \times 10^9 M_\odot$; Assef et al. 2011), Q0957 provides a potentially interesting and important data point for testing models of accretion disk structure. However, the available analyses of Q0957’s only widely-acknowledged microlensing event from 1982–1986 pre-dated the use of the newer, highly quantitative microlensing analysis techniques, and the qualitative methods employed in the published analyses of the event produce either limits or constraints too broad to be informative for current tests of quasar structure and studies of the surface mass density of lens galaxies. For example, Pelt et al. (1998) found that the 1982–1986 microlensing event was consistent with a quasar radius of “roughly” 3×10^{15} cm and could be explained by microlens masses down to $10^{-5} M_\odot$ with only a small fraction ($< 5\%$) in solar mass objects. Refsdal et al. (2000) also analyzed the 1982–1986 microlensing event and subsequent 8-year quiescent period in Q0957 using three different simple lensing mass distribution models, obtaining rough constraints on the range of microlens masses of $10^{-6} < M/M_\odot < 5$ and an upper limit on the size of the quasar’s optical continuum region of $R < 10^{16}$ cm. Attempts to analyze the negligibly low microlensing variability in Q0957’s difference light curve with early numerical simulations (Schmidt & Wambsganss 1998; Wambsganss et al. 2000) could not constrain the quasar size. Such studies could only rule out microlens masses for a given quasar size, and in the end obtained results contradictory to analyses of the 1982–1986 microlensing event. Thus, the lack of unambiguous microlensing events in Q0957 in the relatively recent era of computationally-intensive microlensing analysis has been unfortunate, preventing improved determinations of the quasar’s size and microlens mass properties.

However, as the saying goes, “good things come to those who wait.” In this paper, we combine three new seasons of optical photometric monitoring of Q0957 with previously-published light curves to demonstrate the return of long-time scale uncorrelated variability in the light curves of Q0957. We take advantage of this new microlensing event to place the best constraints yet on the size of the optical accretion disk and the mean mass of the microlenses using the Bayesian Monte Carlo analysis technique of Kochanek (2004). In §2 and §3 we present our new monitoring observations of Q0957 and discuss the methods we use to model the uncorrelated variability in the light curves. We present our results in §4. Throughout our discussion we assume a flat cosmology with $\Omega_M = 0.3$, $\Omega_\Lambda = 0.7$, and $H_0 = 70 \text{ km s}^{-1} \text{ Mpc}^{-1}$ (Hinshaw et al. 2009).

2. OBSERVATIONAL DATA

We regularly monitor the flux of Q0957 A and B in the Sloan Digital Sky Survey r -band using the 1.55-m Kaj Strand Astrometric Reflector at the United States Naval Observatory (USNO), Flagstaff Station, as part of the United States Naval Academy (USNA)/USNO Lensed Quasar Monitoring Program. Our program, which began in 2008, obtains three five-minute exposures of the quasar per night, one night per week on average (weather permitting), using either the Tek2K CCD camera ($0''.33 \text{ pixel}^{-1}$) or the 2048×4096 EEV CCD camera ($0''.18 \text{ pixel}^{-1}$). We present here data taken on 57 nights between 2008 March and 2011 June. The median stellar FWHM (seeing) of the images in our data set is $1''.3$.

We measure the quasar image fluxes using relative photometry. A detailed discussion of our image analysis methods was presented in Kochanek et al. (2006), so we only briefly summarize our procedure here. We treat each quasar image as a point source and model the point spread function with three nested elliptical Gaussian components, keeping the relative astrometry fixed to that derived from *Hubble Space Telescope* (*HST*) images by Keeton et al. (2000) (see Table 1). The $z_l = 0.356$ lens galaxy (Falco et al. 1997) is modeled as a Gaussian approximation to a deVaucouleurs profile for which we fix the effective radius to that derived from the *HST* images of Q0957. The lens galaxy’s flux is held constant in all epochs; we determine the optimal value for the constant flux by repeatedly fitting all the images as a function of lens galaxy flux and finding the value which results in the lowest χ^2 sum over the entire data set. We compare the flux of each quasar image to four reference stars, located at $(-59''.2, -27''.8)$, $(-61''.7, -109''.1)$, $(-68''.5, -89''.8)$, and $(+111''.8, -127''.1)$ relative to Q0957 image A. Because these reference stars are significantly redder than the quasar images ($g - i \sim 0.8 - 0.9$ for the stars and $g - i \sim 0.2$ for the quasar), and the two different detectors used in our USNO program have slightly different spectral responses across the r band, a small color term between the different detectors is introduced into our relative photometry measurements. We determined this color term by fitting the light curves of the quasar images obtained with the EEV camera to the light curves obtained from the Tek2K camera, yielding a magnitude offset of $m_{\text{Tek2K}} - m_{\text{EEV}} = 0.048 \pm 0.002 \text{ mag}$. We apply this correction to the data from the EEV camera, and we include the contribution of the uncertainty in the color term, added in quadrature, in the photometric errors of measurements taken with the EEV camera.

The measurements of Q0957 A and B from our USNO monitoring program are listed in Table 2. We note that we obtained data on two additional epochs which have not been included in Table 2, bringing the total number of observation epochs to 59. However, the images obtained on the two excluded dates were unusable due to high sky brightness levels on one night and corruption of the quasar images by cosmic rays on the other.

In order to obtain a longer time baseline for our microlensing analysis, we have supplemented our new USNO light curves with published monitoring data. We use the R -band photometry from the 0.8-m telescope at the Instituto de Astrofísica de Canarias’ (IAC) Teide Observatory spanning the years 1996–2001 from Serra-Ricart et al. (1999), Oscoz et al. (2001), and Oscoz et al. (2002), deriving the photometric zeropoint offset by comparison to concurrent r -band measurements of image A from Kundić et al. (1997, $\Delta m_{S99-K97} = 0.04$ mag); we neglect the small color term difference between r and R because in our microlensing analysis we use only the relative flux ratio and not the absolute flux. We also use the r -band monitoring data from Shalyapin et al. (2008), spanning the years 2005–2007, and obtain the photometric offset (14.455 ± 0.018 mag) by analyzing their Liverpool Telescope/RATCam images¹ for five different nights with our image analysis procedure and averaging the offsets in magnitude between the published photometry and the values produced by our pipeline. As the frequency of monitoring in those two data sets was nightly, on average, and our monitoring program obtains observations with a frequency closer to weekly, we have averaged the individual measurements into seven-day bins within individual observing seasons, after removing obvious ($> 3\sigma$) outliers in the data set, to prevent those data from having a disproportionate statistical weight relative to the new measurements from USNO. The center of each seven-day bin is defined as the mean HJD of the measurements included in that bin. To serve as errors on these seven-day averages, we compute the standard deviation of the individual data points included in each average. We show the final composite light curves for Q0957A and B from all of the data sources in Figure 1. Unfortunately, we are unable to find any published monitoring data for Q0957 which falls in the gap in Figure 1 between 2001–2005; while the absence of data in this date range will affect our microlensing analysis, we will still derive meaningful results.

We investigated including the two seasons of r -band monitoring from Kundić et al. (1997) from 1995–1996 in our composite light curve for Q0957, which would have extended our time axis even further. However, we chose to not include this data in our analysis because the flux contribution to image B from the lens galaxy has not been subtracted from the photometry in that data set. Moreover, archival images from this data set are no longer available at the Apache Point Observatory or any of its operating consortium institutions, so it was not possible to carry out the deconvolution of image B from the lens galaxy ourselves.

¹Shalyapin et al. have made their monitoring images publicly available at the website <http://dc.zah.uni-heidelberg.de/liverpool/res/rawframes/q/form>.

3. ANALYSIS

3.1. Difference Light Curves and Microlensing Signal

To analyze the light curves of Q0957 for the presence of uncorrelated variability, we must first eliminate the variability intrinsic to the quasar source itself. We accomplish this by first shifting the light curve of image B by the system’s 417-day time delay and then performing a linear interpolation of image B’s shifted light curve to generate a set of photometric measurements at the same epochs of observation as those in image A’s (unshifted) light curve. We discard any data points that were interpolated in the inter-season gaps. Finally, we subtract from the light curve of image A the shifted light curve of image B, creating a time-delay-shifted difference light curve in which only the uncorrelated variability remains.²

In Figure 2 we present the time-delay-shifted difference light curve for Q0957, focusing on the last six years of data. We note in advance that the frequency of observations of Q0957 in the data sets we use does not permit us to confirm or refute the reported observations of intra-day microlensing variability (Colley & Schild 2003). Moreover, the size of the error bars on the measurements render insignificant hints of flux ratio variability on time scales of weeks or months, so we cannot examine reports of the short time scale microlensing variability in Q0957 (Schild 1996; Colley & Schild 2000; Ovaldsen et al. 2003). We do observe a slow but steady brightening of image B relative to image A in the r band, beginning at the start of the Shalyapin et al. (2008) data near MHJD 3650 (in the frame of image A) and continuing to the limit of our USNO data set for image B at MHJD 5311. This clear signature of microlensing is evolving quite slowly, as indicated by the slope of a least-squares straight line fit to the difference light curve of $0.016 \pm 0.006 \text{ mag yr}^{-1}$ (quoted uncertainty is 3σ). Such a slow drift in flux ratio would not have been statistically significant at the time Shalyapin et al. published their data, if even noticeable, as they could only constrain the flux ratio up to date MHJD 3831 in the frame of image A with their data set; our monitoring data from USNO provide the extension in time necessary to confirm that the change in flux ratio is significant in comparison to the observational uncertainties. The duration of the complete microlensing event is presently unclear from the shape of the difference light curve, but the nearly five year span (after time delay correction) so far implies the time scale will be at least that long. We are thus fortunate to be monitoring the first significant multi-year microlensing event in Q0957 in twenty years, and the first to be observed since the system’s time delay was firmly established.

²We note that if we instead shift and interpolate the light curve of image A to the observational epochs of image B, no significant changes in the difference light curve or analysis results are observed.

3.2. Quantitative Monte Carlo Microlensing Analysis

The long time scale and low amplitude of the new microlensing variability are qualitatively consistent with the relatively large optical quasar size predicted by Pelt et al. (1998) and Refsdal et al. (2000) in their analyses of the 1982–1986 microlensing event and are not surprising given that the black hole is very massive. We can place new, improved quantitative constraints on the quasar size and the mass and velocity of the microlenses by analyzing the microlensing variability in our compiled light curve of Q0957 with the techniques described in Kochanek (2004). The analysis method has three major components. First, with the selection of a model for the macroscopic (strong) lensing, a stellar mass function to describe the microlens mass distribution, and an accretion disk model, we generate microlensing magnification patterns for a range of mass contributions from the dark matter halo of the lens galaxy. Next, we use a Monte Carlo method to generate large numbers of trial light curves from the magnification patterns for random source (quasar) trajectories, and fit the simulated light curves to the full observed light curves (years 1995–2011). Finally, we perform a Bayesian statistical analysis on the goodness-of-fit (χ^2) statistics of the light curve fits to calculate probability distributions for accretion disk size, effective source velocity, and mean microlens mass.

To describe the macroscopic lensing in Q0957, we utilize the results from the study of Fadely et al. (2010), who develop detailed models of the quasar lens using as constraints faint knots and structures visible in quasar- and lens-subtracted *HST* images of the strong lensing region as well as the results of weak lensing analysis. The lens potential in Q0957 has been notoriously difficult to model (e.g., Kochanek 1991; Grogin & Narayan 1996; Bernstein & Fischer 1999; Keeton et al. 2000), at least in part due to the two-image nature of the system and the presence of a galaxy cluster surrounding the lens galaxy. Fadely et al. construct a series of models containing an isophotal model of the lens galaxy as the stellar component, a concentric elliptical dark matter halo component representing the lens galaxy and the cluster halo, and a set of general third-order terms in the Taylor series expansion of the potential from the lens environment. Here, we use the convergence (κ) and shear (γ) of the model from Fadely et al. which lies at the peak of the posterior probability distribution to generate the microlensing magnification patterns. So that we may marginalize over the uncertainty in the dark matter fraction in our analysis, we create a series of ten models in which the stellar component of the local convergence κ_* in the vicinity of image B varies linearly in the range $0.1 < (\kappa_*/\kappa)_B < 1.0$. Since image A is much farther from the lens galaxy, we constrain its stellar mass fraction $(\kappa_*/\kappa)_A$ such that the ratio $(\kappa_*/\kappa)_A/(\kappa_*/\kappa)_B$ is held fixed to its value in the Fadely et al. model (~ 0.2). We note that the flux ratio favored by the Fadely et al. models ($f_b/f_a \approx 0.53$) is somewhat lower than what is actually observed in the optical (1.1; Shalyapin et al. 2008; Goicoechea et al. 2005).

The magnification patterns are 4096×4096 images with an outer scale of $20\langle R_E \rangle$, where $\langle R_E \rangle$ is the Einstein radius for the mean microlens mass $\langle M \rangle$ projected into the source plane. The outer dimension and pixel scale are chosen to be sufficiently large to representatively sample the magnification patterns and sufficiently small to resolve the accretion disk. The stellar mass function we use to generate the population of microlenses for the patterns is a power law, $dN/dM \propto M^{-1.3}$, with a ratio of maximum-to-minimum mass (dynamic range) of 50. This function reasonably approximates the Galactic disk mass function of Gould (2000); assuming a different mass function (such as that of Salpeter 1955) will have a negligible effect on our results due to the other, larger sources of uncertainty (see, e.g., Paczyński 1986; Wyithe et al. 2000). We create four independent magnification patterns for each quasar image for all ten evenly spaced stellar mass fractions.

Because the effects of finite continuum source size are generally not negligible for quasar microlensing, we convolve the magnification patterns with the surface brightness profile of the source for a grid of source sizes before computing trial light curves. We model the accretion disk as a face-on, thin disk radiating as a blackbody with a power-law temperature profile $T \propto R^{3/4}$. The scale radius of the disk, r_s , is defined as the radius at which the disk temperature matches the rest-frame wavelength of the filter used in our monitoring observations, $kT = hc/\lambda_{\text{rest}}$ (for r -band monitoring of Q0957, $\lambda_{\text{rest}} = 2593 \text{ \AA}$). Our model matches the outer regions of the thin disk model of Shakura & Sunyaev (1973), but we neglect the drop in temperature in the center due to the inner edge of the disk and the correction factor from general relativity to avoid introducing additional parameters. The effect of the simplification on our result for the accretion disk size is small compared to the uncertainties in other parameters, as long as the disk is significantly larger than the radius of the inner disk edge (Dai et al. 2010). We caution that because microlensing amplitude depends on the projected area of the source and not its shape, and because we assume a face-on disk model, the disk radius we infer will be an effective radius defined as the radius of a circle of the same projected area as the accretion disk. The true radius will be $(\cos i)^{-1/2}$ times this effective radius, where i is the inclination of the disk.

We generate 10^6 trial light curves for each of the 40 sets of magnification patterns. In each realization we randomly select an initial position and effective velocity for the source trajectory, assuming the values are independent and uniformly distributed. As in Kochanek (2004), we neglect the motion of the stars within the lens galaxy and describe the observer’s motion as the projection of the CMB dipole velocity onto the lens plane. We then use Bayesian methods to analyze the χ^2 statistics of the many light curve fits and calculate likelihood functions for the quasar source size and velocity in Einstein units (\hat{r}_s and \hat{v}_e) since all results scale with the unknown mass of an average microlens $\langle M \rangle$. We estimate the true, unscaled physical source size $r_s = \hat{r}_s \langle M/M_\odot \rangle^{1/2}$ and mean microlens mass $\langle M \rangle$ by combining

the probability distributions of the scaled source size, $P(\hat{r}_s)$, and the scaled effective velocity, $P(\hat{v}_e)$, obtained from the Bayesian analysis with a prior probability function for the true, unscaled effective source velocity, $P(v_e)$. We construct $P(v_e)$ using the method described in Kochanek (2004), applying the measured stellar velocity dispersion for the lens galaxy ($\sigma_* = 288 \pm 9 \text{ km s}^{-1}$; Tonry & Franx 1999), and obtaining the dispersion of the peculiar velocity distribution at the redshifts of Q0957 and the lens galaxy from the power-law fits by Mosquera & Kochanek (2011) to the peculiar velocity models of Tinker et al. (2011, in preparation).

4. RESULTS AND DISCUSSION

In Figure 3 we show the probability distribution for the scaled effective source plane (Einstein) velocity \hat{v}_e resulting from the Bayesian analysis of our Monte Carlo light curve simulations, along with the probability density for the true source velocity, $P(v_e)$, used to determine the mean microlens mass $\langle M \rangle$ and physical source size r_s . The \hat{v}_e distribution has a median of 1600 km s^{-1} and is wide, with 68% confidence range of $600 \text{ km s}^{-1} < \hat{v}_e < 3500 \text{ km s}^{-1}$. The distribution is also visibly asymmetric, with a substantial low-velocity tail. The width and asymmetry indicate the wide range of feasible solutions to the microlensing variability in Q0957 and reflect the ease with which the system’s light curve was fit by the Monte Carlo code. Because the Monte Carlo simulations produce large numbers of acceptable fits and the χ^2 per degree of freedom for the best fits tends to be quite low (~ 0.4) even with insignificant (small) assumed values for the systematic errors of the flux ratio and photometry, we conclude that the spread in the velocity distribution is a consequence of the low intrinsic variability of Q0957 coupled with the very low amplitude of the microlensing signal, making the light curve simple to reproduce. An additional factor may be that the lack of observational constraints in the four-year gap in the compiled light curve permits considerable freedom in model behavior, as shown in Figure 4. We tested this hypothesis by conducting an experiment in which we forced the flux ratio in the gap to stay within $\pm 0.05 \text{ mag}$ of its mean value in the dates bracketing the gap, $(m_A - m_B) = 0.04 \pm 0.03 \text{ mag}$. The experiment resulted in a minor narrowing of the \hat{v}_e distribution, but the change was not significant enough to justify any firm conclusions about the influence of the gap on our results.

Because the mean microlens mass is proportional to the inverse square of the scaled effective velocity ($\hat{v}_e = v_e \langle M/M_\odot \rangle^{-1/2}$), the broad range in permitted velocities causes the mean mass to be poorly constrained, which is apparent in the probability distribution for $\langle M/M_\odot \rangle$ shown in the right panel of Figure 3. The median of the $\langle M/M_\odot \rangle$ distribution is

$0.2 M_\odot$, with a 68% confidence range of $0.02 M_\odot < \langle M \rangle < 1.3 M_\odot$. Our estimate of the mean microlens mass is appropriate for stars in an old elliptical galaxy, and falls well within the most probable range found by Refsdal et al. (2000) of $10^{-6} < M/M_\odot < 5$. Our constraints do not permit a dominant population of planetary and sub-planetary mass ($< 10^{-3} M_\odot$), compact microlenses in the lens galaxy, consistent with the results of Schmidt & Wambsganss (1998) and Wambsganss et al. (2000). Our new constraints are also not consistent with the result of Pelt et al. (1998) for the 1982–1986 event, in which a significant population of stellar mass microlenses is ruled out. However, as our microlensing analysis technique is significantly more sophisticated than that used in earlier studies and does not rely on the assumption of a single value for the source size or effective velocity to derive the microlens mass, we consider our new result to be much more robust.

While we have attempted to constrain the stellar-to-dark mass fraction κ_*/κ in the lens galaxy of the Q0957 system, the probability distribution resulting from our Bayesian analysis is uninformative, with no strong peaks or trends favoring any particular κ_*/κ value. We suspect that the primary reason for this failure is that there is insufficient uncorrelated variability in the light curves of Q0957 to constrain the dark matter fraction. However, the addition of X-ray data to the microlensing analysis may provide stronger constraints, as it has in the case of PG 1115+080 (Morgan et al. 2008; Pooley et al. 2009) and RXJ 1131-1231 (Dai et al. 2010).

In Figure 5 we show the probability distribution for the physical source size r_s of the quasar’s accretion disk in the observed-frame r -band which results from our microlensing analysis. The distribution as shown has not been corrected for inclination i ; however, in the text that follows all the numerical quantities we discuss will be corrected by a factor of $(\cos i)^{-1/2}$ assuming an inclination of 60° , the expectation value of a random distribution of inclinations. Note that the thin disk scale radius can be converted to a half-light radius using the relation $r_{1/2} = 2.44 r_s$. The median of the microlensing thin-disk size distribution is $\log(r_s/\text{cm}) = 16.2 \pm 0.5$, where the error bar represents the bounds of the 68% confidence interval. When converted to a half-light radius, which is comparable between different source models (Mortonson et al. 2005), the source size we obtain from our analysis [$\log(r_{1/2}/\text{cm}) = 16.5 \pm 0.5$] appears to be marginally consistent with the R -band half-light radii (converted from σ of a Gaussian disk profile) obtained by Pelt et al. (1998, $10^{15.5} \text{ cm}$) and Refsdal et al. (2000, $< 10^{16.1} \text{ cm}$) from the data set covering the 1982–1986 microlensing event and the following 8 years of stable flux ratio. We note that our source size result is substantially larger than those used by Schmidt & Wambsganss (1998) and Wambsganss et al. (2000) to constrain the microlens mass distribution [$\log(r_s/\text{cm}) < 14.2$]; yet our mean microlens mass is still consistent with their constraints. We also experimented with the use of a uniform prior on the microlens mass of $0.1 < \langle M/M_\odot \rangle < 1.0$. Although the median of the resulting r_s

distribution is essentially the same as that found without imposing the mass prior, within the uncertainties, the distribution yielded by the prior contains a small but significant probability in solutions with small source sizes which are not physically reasonable. We suspect that the occurrence of this “shelf” at the low end of the size distribution is an artifact of a combination of the paucity of microlensing variability in the observations and the mass prior itself. By limiting $\langle M \rangle$ to a range about which its distribution (derived from the v_e prior) is not symmetric, we give more statistical weight to solutions from one side of the distribution. Since the Einstein velocity (\hat{v}_e) scale implied by a given microlens mass scales as $\hat{v}_e = v_e \langle M/M_\odot \rangle^{-1/2}$, the solutions with very low Einstein velocities are given more weight relative to the highest velocity solutions when the prior is applied. In the case of Q0957, the solutions with low Einstein velocity correspond preferentially to small source sizes; however, at very small sizes all solutions become equally likely since none of them pass near a caustic.

Morgan et al. (2010) used the same microlensing analysis technique as we use here on light curves of a sample of 11 different gravitationally lensed quasars to show that the quasar accretion disk size at 2500 Å inferred from microlensing (r_{2500}) is correlated with central black hole mass as $r_{2500} \propto M_{\text{BH}}^{0.80 \pm 0.17}$. Although the scaling of the observed correlation is consistent within the uncertainties with thin disk theory ($R \propto M_{\text{BH}}^{2/3}$), the correlation implies a quasar radiative efficiency η that is approximately an order of magnitude lower than is expected based on the local supermassive black hole mass and quasar luminosity functions. We can use this r_{2500} – M_{BH} correlation as an independent check on our assertion that the uncorrelated variability we have observed in Q0957 is a result of microlensing. To scale the observed-frame r -band source size we find for Q0957 to a rest-frame wavelength of 2500 Å, we assume the $R \propto \lambda^{4/3}$ scaling of thin disk theory which is supported by several observational studies of quasar microlensing (e.g., Anguita et al. 2008; Poindexter et al. 2008; Floyd et al. 2009; Mosquera et al. 2011). In doing so, we note that the effect of the wavelength scaling is minimal for Q0957 since the effective wavelength of the observed-frame r filter corresponds to 2593 Å at $z = 1.41$. For the black hole mass we use the C IV emission-line estimate of Assef et al. (2011), which has an associated systematic uncertainty of 0.33 dex. In Figure 6, we place Q0957 on the best-fit r_{2500} – M_{BH} relation found by Morgan et al., along with the quasar data points used to derive the correlation. Q0957 is consistent with the relation; the agreement supports our assertion that microlensing is the source of the quasar’s long-timescale uncorrelated variability.

Similarly to Morgan et al. (2010), we also show for comparison in Figure 6 quasar source sizes calculated by two additional methods. First, we calculate the theoretical scale radius of a thin accretion disk at a rest wavelength of 2500 Å from its central black hole mass (“theory size”) using Eq. 2 of Morgan et al., and assuming accretion efficiency $\eta = 0.1$ and Eddington ratio $L/L_E = 1/3$ (Kollmeier et al. 2006). Second, we calculate the disk size under the

thin disk model (a blackbody with a $T \propto R^{-3/4}$ temperature profile) constrained by the observed magnification-corrected optical flux/luminosity from *HST* F814W measurements (“flux size”, see Eq. 3 of Morgan et al.). When we compare the results of the different methods of size calculation for Q0957, we observe that the microlensing size is larger than the theory size, also noted for other lensed quasars by Morgan et al. (2010) and Blackburne et al. (2011). Pooley et al. (2007) arrive at a similar conclusion, although they use bolometric luminosity-based black hole masses to calculate their theory sizes which are thus more similar to our flux sizes. Furthermore, the microlensing size for Q0957 is larger than its flux size as well, which was also found by Morgan et al. and Mediavilla et al. (2011) for their respective quasar samples. However, the significance of the discrepancy we find for Q0957 is not as large as that typically found by Blackburne et al. (2011) for their sample: while they rule out the black hole mass-based theoretical prediction by at least 3σ in nearly every case, the flux size for Q0957 falls within the 68% confidence interval (essentially 1σ) of the microlensing size, and the theory size within the 80% confidence interval ($\sim 1.3\sigma$). While this may simply reflect the relatively large uncertainty in the microlensing size estimate for Q0957 compared to other microlensed quasars, it is also possible that the difference in significance is related to our different treatment of systematic errors from the analysis of Blackburne et al. The origin of the discrepancies between the microlensing size, theory size, and flux size remain unclear. As Morgan et al. and Blackburne et al. point out, adjusting the mass accretion rate ($L/\eta L_E$) of Q0957 by lowering η or using a higher-than-typical Eddington ratio may resolve the discrepancy of the theory size with the microlensing size, but such adjustments will not address the fact that the flux size is smaller than the microlensing size.

One possible explanation for the size discrepancy is that the observed r -band flux may be contaminated by (a) UV/optical light from the continuum source scattered by the broad-line region (BLR); or (b) higher energy continuum emission reprocessed by the BLR and re-emitted as UV/optical emission lines. Contamination from line emission is an especially strong concern for our observations of Q0957 because the quasar’s redshifted Mg II line falls within the r bandpass and could cause us to overestimate the microlensing size. Thus, it is important that we consider contamination scenarios in our analysis. So, we have repeated our Monte Carlo light curve simulations assuming that different percentages of the observed r -band flux can be attributed to unmicrolensed contamination from the BLR. When we do so, we find that if we assume 10% contamination we still obtain a median physical accretion disk size in r -band of $\log(r_{s,10}/\text{cm}) = 16.1 \pm 0.5$. Even when we assume a 30% contribution to the observed flux from contamination, we obtain $\log(r_{s,30}/\text{cm}) = 16.0^{+0.5}_{-0.4}$, insignificantly different from our original microlensing size. Thus, neither scattering nor line contamination appear to produce a significant effect on the microlensing size result, relative to our other sources of uncertainty. Moreover, even if line contamination produced a significant decrease

in the microlensing size, the flux size would be reduced along with the microlensing size, and the two would still not be reconciled.

Although we are not able to resolve the discrepancy between the different accretion disk size estimates and our microlensing size measurement, we are nonetheless very encouraged to observe a long-term microlensing event in a quasar at the high end of the black hole mass function. Moreover, Q0957 is relatively easy to monitor with ground-based observatories, since the quasar images and lens galaxy are relatively widely separated and the time delay is well-determined. Future multi-wavelength optical monitoring as well as X-ray monitoring will be most informative to examine the temperature profile of the accretion disk and compare the X-ray and optical sizes.

The authors wish to thank L. Goicoechea, E. Turner, & R. McMillan for their assistance in obtaining historical photometric data for Q0957. We also thank the anonymous referee for suggestions which improved the data presented in this paper. This material is based upon work supported by the National Science Foundation under grant No. AST-0907848 (to C.W.M.), AST-0708082, and AST-1009756 (to C.S.K.). C.W.M. also gratefully acknowledges support from the Research Corporation for Science Advancement and Chandrasekhar X-Ray Center award 11700501.

REFERENCES

- Anguita, T., et al. 2008, *A&A*, 480, 327
- Assef, R. J., et al. 2011, *ApJ*, in press
- Bate, N. F., Webster, R. L., & Wyithe, J. S. B. 2007, *MNRAS*, 381, 1591
- Bernstein, G., & Fischer, P. 1999, *AJ*, 118, 14
- Blackburne, J. A., Pooley, D., Rappaport, S., & Schechter, P. L. 2011, *ApJ*, 729, 34
- Chang, K., & Refsdal, S. 1979, *Nature*, 282, 561
- Colley, W. N., & Schild, R. S. 2000, *ApJ*, 540, 104
- Colley, W. N., & Schild, R. S. 2003, *ApJ*, 594, 97
- Dai, X., Kochanek, C. S., Chartas, G., Kozłowski, S., Morgan, C. W., Garmire, G., & Agol, E. 2010, *ApJ*, 709, 278
- Eigenbrod, A., Courbin, F., Meylan, G., Agol, E., Anguita, T., Schmidt, R. W., & Wambsganss, J. 2008, *A&A*, 490, 933
- Fadely, R., Keeton, C. R., Nakajima, R., & Bernstein, G. M. 2010, *ApJ*, 711, 246
- Falco, E. E., Shapiro, I. I., Moustakas, L. A., & Davis, M. 1997, *ApJ*, 484, 70
- Floyd, D. J. E., Bate, N. F., & Webster, R. L. 2009, *MNRAS*, 398, 233
- Gil-Merino, R., Goicoechea, L. J., Serra-Ricart, M., Oscoz, A., Alcalde, D., & Mediavilla, E. 2001, *MNRAS*, 322, 397
- Goicoechea, L. J., et al. 2005, *ApJ*, 619, 19
- Gould, A. 2000, *ApJ*, 535, 928
- Grogin, N. A., & Narayan, R. 1996, *ApJ*, 464, 92
- Hinshaw, G., et al. 2009, *ApJS*, 180, 225
- Keeton, C. R., et al. 2000, *ApJ*, 542, 74
- Kochanek, C. S. 1991, *ApJ*, 382, 58
- Kochanek, C. S. 2004, *ApJ*, 605, 58

- Kochanek, C. S., Morgan, N. D., Falco, E. E., McLeod, B. A., Winn, J. N., Dembicky, J., & Ketzeback, B. 2006, *ApJ*, 640, 47
- Kollmeier, J. A., et al. 2006, *ApJ*, 648, 128
- Kundić, T., et al. 1997, *ApJ*, 482, 75
- Mediavilla, E., et al. 2009, *ApJ*, 706, 1451
- Mediavilla, E., et al. 2011, *ApJ*, 730, 16
- Morgan, C. W., Kochanek, C. S., Dai, X., Morgan, N. D., & Falco, E. E. 2008, *ApJ*, 689, 755
- Morgan, C. W., Kochanek, C. S., Morgan, N. D., & Falco, E. E. 2010, *ApJ*, 712, 1129
- Mortonson, M. J., Schechter, P. L., & Wambsganss, J. 2005, *ApJ*, 628, 594
- Mosquera, A. M., Muñoz, J. A., & Mediavilla, E. 2009, *ApJ*, 691, 1292
- Mosquera, A. M., & Kochanek, C. S. 2011, *ApJ*, 738, 96
- Mosquera, A. M., Muñoz, J. A., Mediavilla, E., & Kochanek, C. S. 2011, *ApJ*, 728, 145
- Oscos, A., Alcalde, D., Serra-Ricart, M., et al. 2001, *ApJ*, 552, 81
- Oscos, A., Alcalde, D., Serra-Ricart, M., Mediavilla, E., & Muñoz, J. A. 2002, *ApJ*, 573, L1
- Ovaldsen, J. E., Teuber, J., Schild, R. E., & Stabell, R. 2003, *A&A*, 402, 891
- Paczynski, B. 1986, *ApJ*, 301, 503
- Pelt, J., Schild, R., Refsdal, S., & Stabell, R. 1998, *A&A*, 336, 829
- Poindexter, S., Morgan, N. D., & Kochanek, C. S. 2008, *ApJ*, 673, 34
- Pooley, D., Blackburne, J. A., Rappaport, S., & Schechter, P. L. 2007, *ApJ*, 661, 19
- Pooley, D., Rappaport, S., Blackburne, J., Schechter, P. L., Schwab, J., & Wambsganss, J. 2009, *ApJ*, 697, 1892
- Refsdal, S., Stabell, R., Pelt, J., & Schild, R. 2000, *A&A*, 360, 10
- Salpeter, E. E. 1955, *ApJ*, 121, 161
- Schild, R. E. 1990, *AJ*, 100, 1771

- Schild, R. E. 1996, *ApJ*, 464, 125
- Schmidt, R. W., & Wambsganss, J. 1998, *A&A*, 335, 379
- Schmidt, R. W., & Wambsganss, J. 2010, *GReGr*, 42, 2127
- Serra-Ricart, M., et al. 1999, *ApJ*, 526, 40
- Shakura, N. I., & Sunyaev, R. A. 1973, *A&A*, 24, 337
- Shalyapin, V. N., Goicoechea, L. J., Koptelova, E., Ullán, A., & Gil-Merino, R. 2008, *A&A*, 492, 401
- Tonry, J. L., & Franx, M. 1999, *ApJ*, 515, 512
- Vanderriest, C., Schneider, J., Herpe, G., Chevreton, M., Moles, M., & Wlérick, G. 1989, *A&A*, 215, 1
- Walsh, D., Carswell, R. F., & Weymann, R. J. 1979, *Nature*, 279, 381
- Wambsganss, J., Schmidt, R. W., Colley, W., Kundić, T., & Turner, E. L. 2000, *A&A*, 362, L37
- Wyithe, J. S. B., Webster, R. L., & Turner, E. L. 2000, *MNRAS*, 315, 51

Table 1. *HST* Astrometry and Photometry of Q 0957+561

Component	Astrometry		Photometry		
	Δ R.A. (arcsec)	Δ Dec. (arcsec)	F555W (mag)	F814W (mag)	F160W (mag)
A	$\equiv 0$	$\equiv 0$	17.09 ± 0.07	16.71 ± 0.05	15.60 ± 0.03
B	$+1.229 \pm 0.005$	-6.048 ± 0.004	17.11 ± 0.05	16.78 ± 0.04	15.68 ± 0.03
Lens Galaxy	$+1.406 \pm 0.006$	-5.027 ± 0.005	19.05 ± 0.04	17.12 ± 0.02	15.14 ± 0.09

Note. — *HST* astrometry and photometry for Q0957 are taken from Keeton et al. (2000).

Table 2. Q 0957+561 Light Curves

HJD - 2450000 (days)	Seeing (arcsec)	QSO A (mag)	QSO B (mag)	$\langle \text{Stars} \rangle$ (mag)
4554.712	1.3	2.671 ± 0.004	2.419 ± 0.004	0.013 ± 0.002
4555.767	1.4	2.659 ± 0.004	2.412 ± 0.004	0.010 ± 0.002
4561.722	1.3	2.665 ± 0.004	2.417 ± 0.004	0.013 ± 0.002
4570.669	1.5	2.669 ± 0.004	2.413 ± 0.004	-0.004 ± 0.002
4584.677	1.4	2.664 ± 0.004	2.378 ± 0.004	0.008 ± 0.002
4596.704	1.4	2.682 ± 0.004	2.377 ± 0.005	-0.002 ± 0.002
4613.691	1.4	2.689 ± 0.004	2.392 ± 0.004	0.008 ± 0.002
4617.702	1.3	2.691 ± 0.004	2.412 ± 0.004	0.010 ± 0.002
4793.005	0.9	2.733 ± 0.004	2.541 ± 0.005	0.007 ± 0.002
4802.980	1.4	2.711 ± 0.005	2.544 ± 0.005	-0.008 ± 0.002
4807.929	1.3	2.728 ± 0.005	2.563 ± 0.005	-0.002 ± 0.002
4829.857	1.3	2.747 ± 0.004	2.604 ± 0.004	0.007 ± 0.002
4833.894	1.4	2.726 ± 0.004	2.603 ± 0.004	0.006 ± 0.002
4839.966	1.6	2.722 ± 0.005	2.608 ± 0.005	-0.017 ± 0.002
4846.758	1.8	2.730 ± 0.004	2.621 ± 0.004	-0.011 ± 0.002
4862.882	1.2	2.706 ± 0.004	2.631 ± 0.004	0.013 ± 0.002
4877.716	2.0	2.684 ± 0.004	2.618 ± 0.004	-0.009 ± 0.002
4883.932	1.1	2.673 ± 0.002	2.624 ± 0.002	-0.078 ± 0.002
4891.824	1.3	2.635 ± 0.004	2.625 ± 0.004	0.054 ± 0.001
4911.800	1.1	2.618 ± 0.004	2.665 ± 0.004	0.013 ± 0.002
4942.797	1.7	2.573 ± 0.003	2.655 ± 0.004	0.011 ± 0.001
4964.715	1.2	2.587 ± 0.004	2.630 ± 0.004	0.013 ± 0.001
4981.695	2.2	2.580 ± 0.005	2.608 ± 0.005	-0.028 ± 0.002
4997.677	1.2	2.608 ± 0.004	2.626 ± 0.004	0.013 ± 0.002
5144.981	1.3	2.573 ± 0.004	2.656 ± 0.004	0.004 ± 0.002
5157.964	1.1	2.578 ± 0.004	2.642 ± 0.004	0.001 ± 0.002
5186.024	1.2	2.558 ± 0.004	2.603 ± 0.004	0.005 ± 0.002
5201.946	1.2	2.579 ± 0.004	2.639 ± 0.004	0.003 ± 0.002
5208.993	1.2	2.585 ± 0.004	2.652 ± 0.004	0.009 ± 0.002
5241.874	2.1	2.627 ± 0.004	2.668 ± 0.004	-0.010 ± 0.002
5261.687	1.4	2.631 ± 0.004	2.667 ± 0.005	-0.016 ± 0.002
5296.691	0.8	2.641 ± 0.004	2.617 ± 0.004	0.015 ± 0.002

Table 2—Continued

HJD - 2450000 (days)	Seeing (arcsec)	QSO A (mag)	QSO B (mag)	$\langle \text{Stars} \rangle$ (mag)
5311.690	1.3	2.634 ± 0.004	2.575 ± 0.005	-0.011 ± 0.002
5320.745	0.9	2.639 ± 0.004	2.546 ± 0.004	0.017 ± 0.001
5324.729	0.7	2.636 ± 0.004	2.536 ± 0.004	0.018 ± 0.001
5332.717	1.1	2.630 ± 0.004	2.528 ± 0.004	0.065 ± 0.002
5348.695	1.1	2.605 ± 0.004	2.480 ± 0.004	0.013 ± 0.001
5352.685	0.9	2.596 ± 0.004	2.483 ± 0.004	0.014 ± 0.002
5358.688	1.8	2.560 ± 0.004	2.463 ± 0.005	-0.003 ± 0.002
5506.991	1.4	2.650 ± 0.004	2.474 ± 0.004	0.007 ± 0.002
5519.030	0.9	2.712 ± 0.003	2.490 ± 0.003	-0.008 ± 0.001
5527.937	1.7	2.692 ± 0.004	2.483 ± 0.004	-0.008 ± 0.002
5535.032	1.1	2.704 ± 0.006	2.489 ± 0.006	-0.016 ± 0.002
5543.989	1.0	2.713 ± 0.004	2.497 ± 0.004	0.014 ± 0.002
5563.958	1.3	2.705 ± 0.004	2.477 ± 0.004	0.009 ± 0.001
5590.779	1.0	2.729 ± 0.004	2.496 ± 0.004	0.017 ± 0.001
5604.847	1.5	2.711 ± 0.004	2.465 ± 0.004	0.004 ± 0.002
5621.687	1.0	2.705 ± 0.004	2.482 ± 0.004	0.012 ± 0.002
5626.779	1.2	2.698 ± 0.005	2.487 ± 0.005	0.003 ± 0.002
5649.715	1.1	2.661 ± 0.004	2.538 ± 0.004	0.015 ± 0.001
5653.710	1.1	2.659 ± 0.004	2.545 ± 0.004	0.014 ± 0.001
5664.750	1.2	2.658 ± 0.004	2.559 ± 0.004	0.003 ± 0.002
5674.748	1.6	2.648 ± 0.008	2.566 ± 0.008	-0.091 ± 0.003
5684.672	1.3	2.653 ± 0.004	2.564 ± 0.004	-0.007 ± 0.001
5702.677	1.7	2.663 ± 0.004	2.572 ± 0.004	0.005 ± 0.002
5712.673	1.0	2.671 ± 0.004	2.582 ± 0.004	0.012 ± 0.002
5733.651	1.2	2.673 ± 0.005	2.566 ± 0.005	-0.065 ± 0.002

Note. — HJD is the Heliocentric Julian Day. The magnitudes listed in the QSO A and B columns are measured relative to the comparison stars. The magnitudes in the $\langle \text{Stars} \rangle$ column are the mean magnitudes of the comparison stars for that epoch relative to their mean over all epochs.

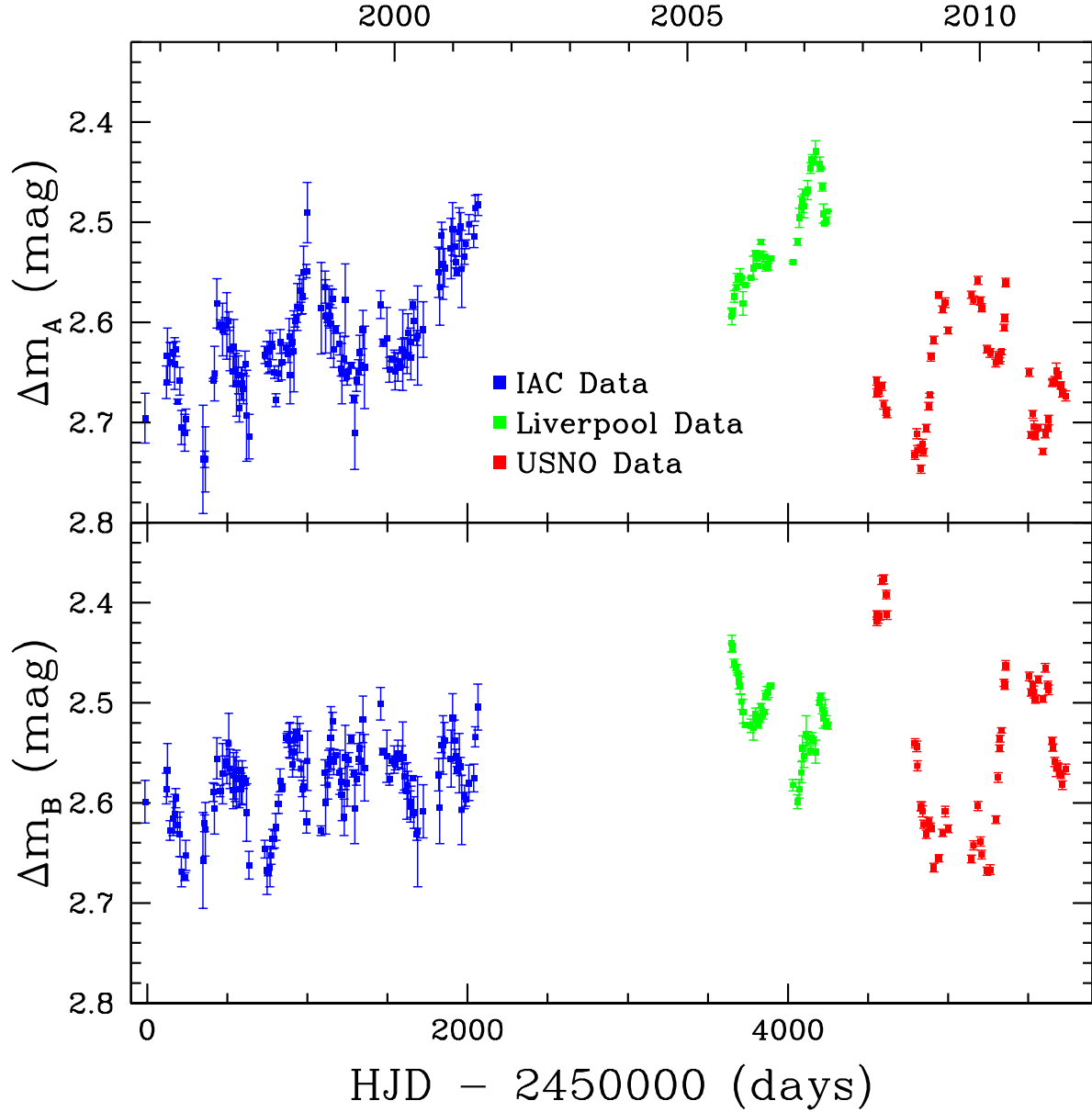


Fig. 1.— Composite r -band light curve of Q0957 including historical measurements from Serra-Ricart et al. (1999, IAC data), Oscoz et al. (2001, 2002, IAC data), Shalyapin et al. (2008, Liverpool data), and our new USNO data. The ~ 1600 day gap in the center of the light curve reflects an absence of published photometric monitoring for this system, but will not prevent us from deriving useful constraints from our microlensing analysis.

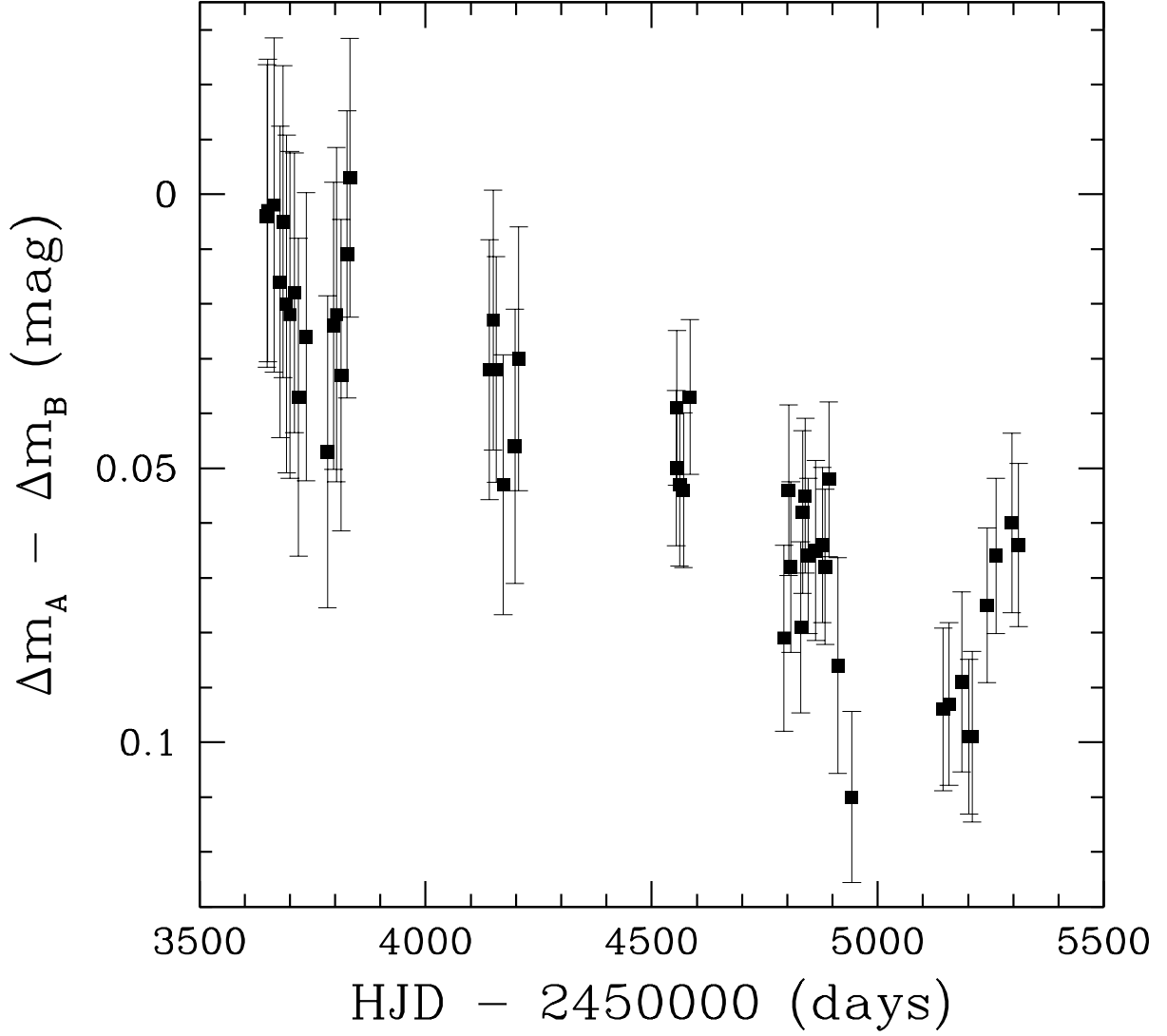


Fig. 2.— Time-shifted difference light curve of Q0957 from 2005–2010, displaying the slow increase in flux ratio of images A and B over five years that is a clear signature of microlensing. A simple linear fit to the observed data points indicates an average change of $\sim 0.02 \text{ mag yr}^{-1}$.

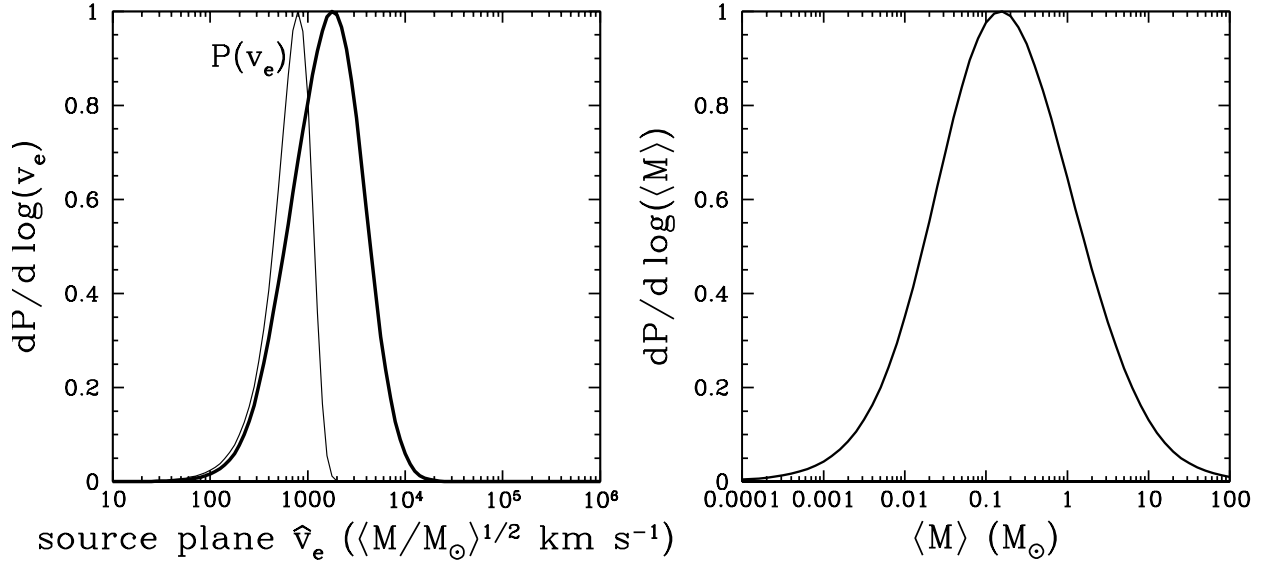


Fig. 3.— *Left panel*: Probability distribution for the effective source velocity \hat{v}_e for Q0957. The heavy line is the scaled effective velocity distribution in Einstein units, which has median $\hat{v}_e = 1600$ km s $^{-1}$, while the light line indicates the prior probability distribution for the true source velocity. *Right panel*: Probability distribution for the mean microlens mass $\langle M \rangle$ for the lens galaxy in the Q0957 system, which has a median value of $\langle M \rangle = 0.2 M_\odot$. $\langle M \rangle$ is calculated by combining the scaled effective source velocity distribution with the prior probability distribution for the true source velocity. The width of the $\langle M \rangle$ distribution reflects the uncertainty in the effective velocity apparent in the left panel, since $\langle M \rangle$ depends on the inverse square of the scaled effective velocity \hat{v}_e .

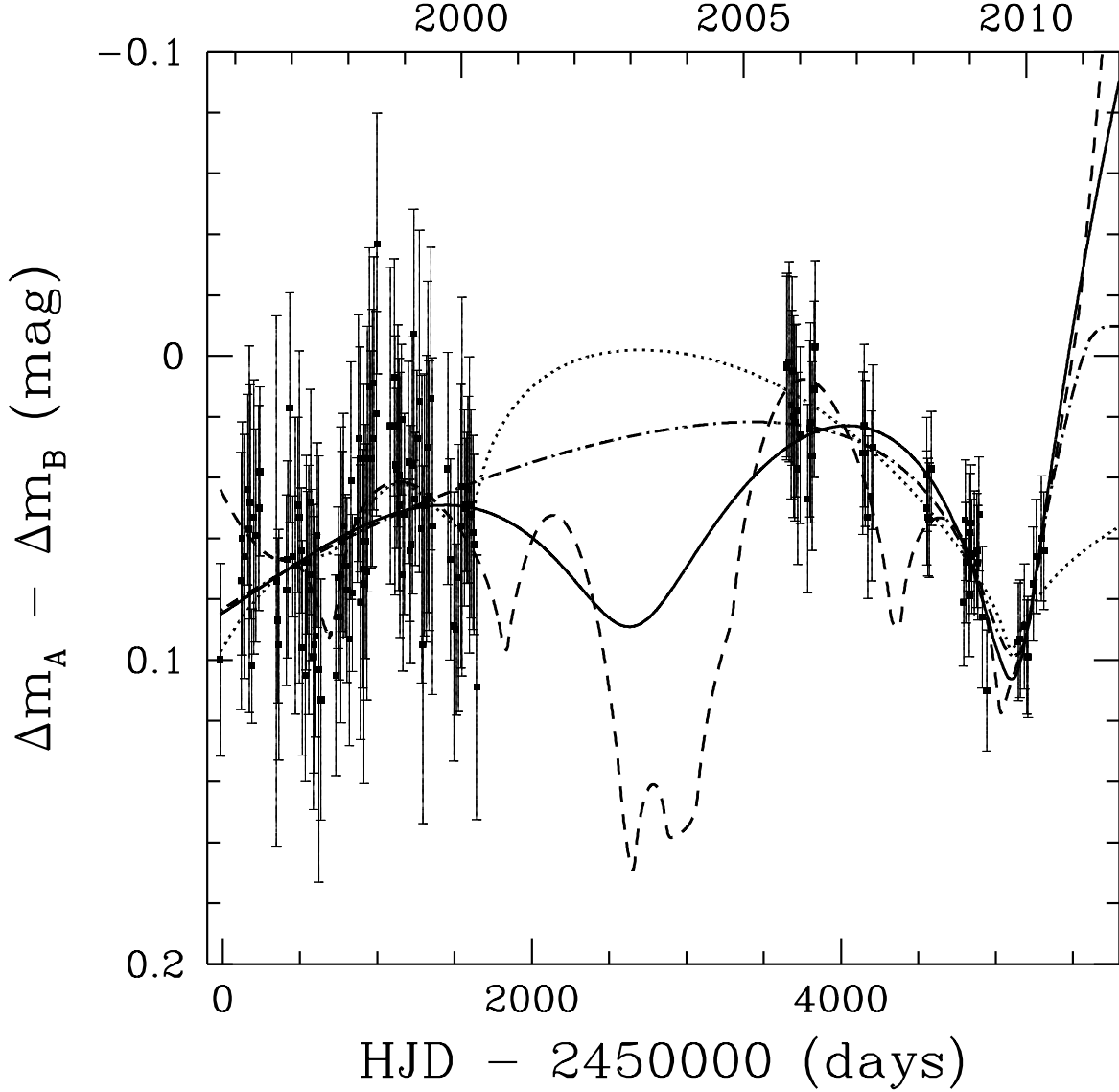


Fig. 4.— Time-shifted difference light curve of Q0957 with a variety of simulated light curves that are good fits to the observed data, illustrating the ease with which the observed data are fit with simulated microlensing trajectories for a variety of different physical parameters. The different line types correspond to simulations with $\kappa_*/\kappa = 0.1$ and $\hat{v}_e = 1468 \text{ km s}^{-1}$ (solid line), $\kappa_*/\kappa = 0.5$ and $\hat{v}_e = 561 \text{ km s}^{-1}$ (dotted line), $\kappa_*/\kappa = 0.8$ and $\hat{v}_e = 344 \text{ km s}^{-1}$ (dashed line), and $\kappa_*/\kappa = 0.3$ and $\hat{v}_e = 2082 \text{ km s}^{-1}$ (dot-dashed line).

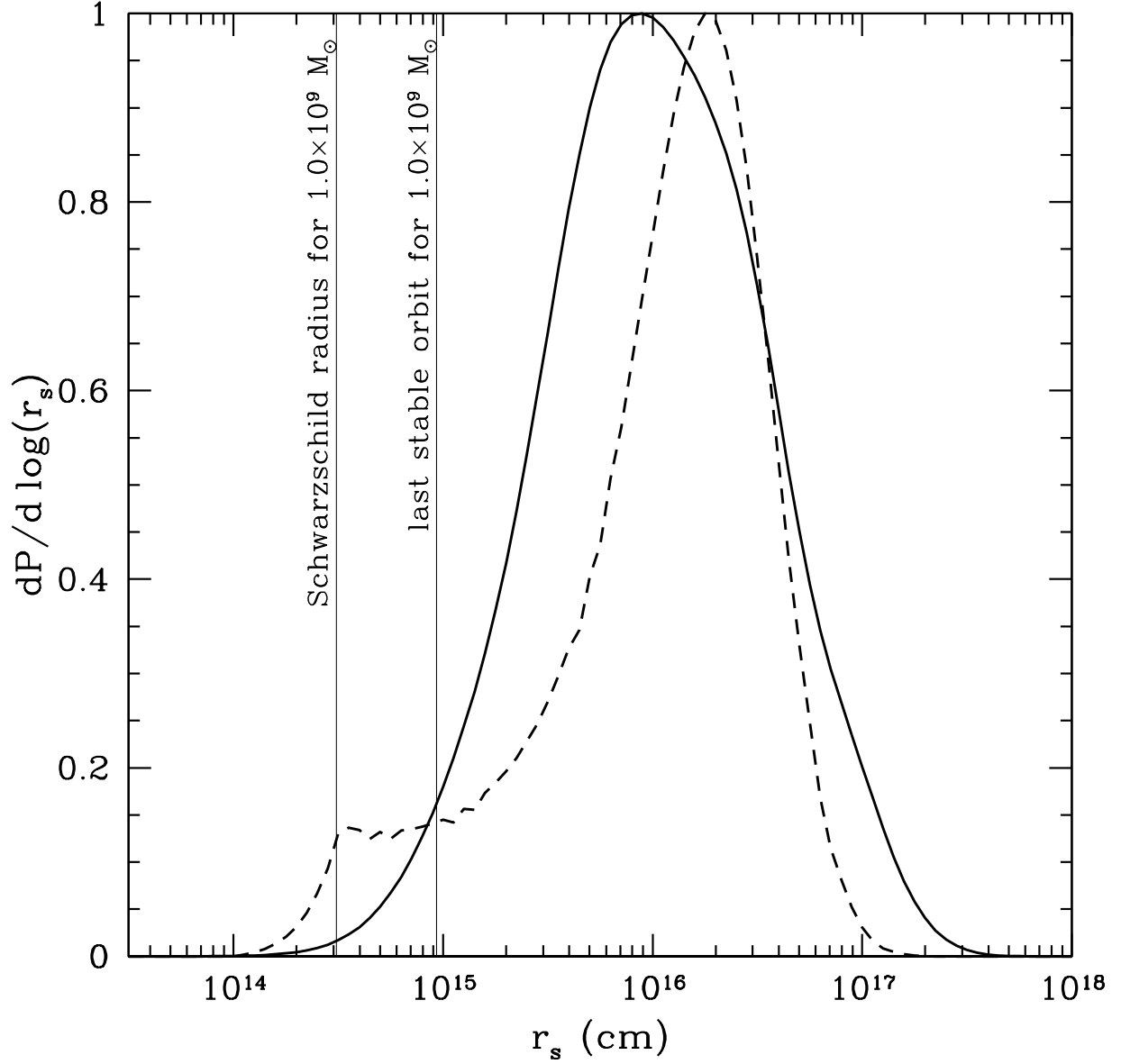


Fig. 5.— Relative probability distribution for the physical thin disk scale size r_s for Q0957. The solid line represents the probability distribution directly arising from the microlensing simulations, while the dashed line shows the result of imposing a prior on the mean microlens mass of $0.1 < \langle M/M_\odot \rangle < 1.0$.

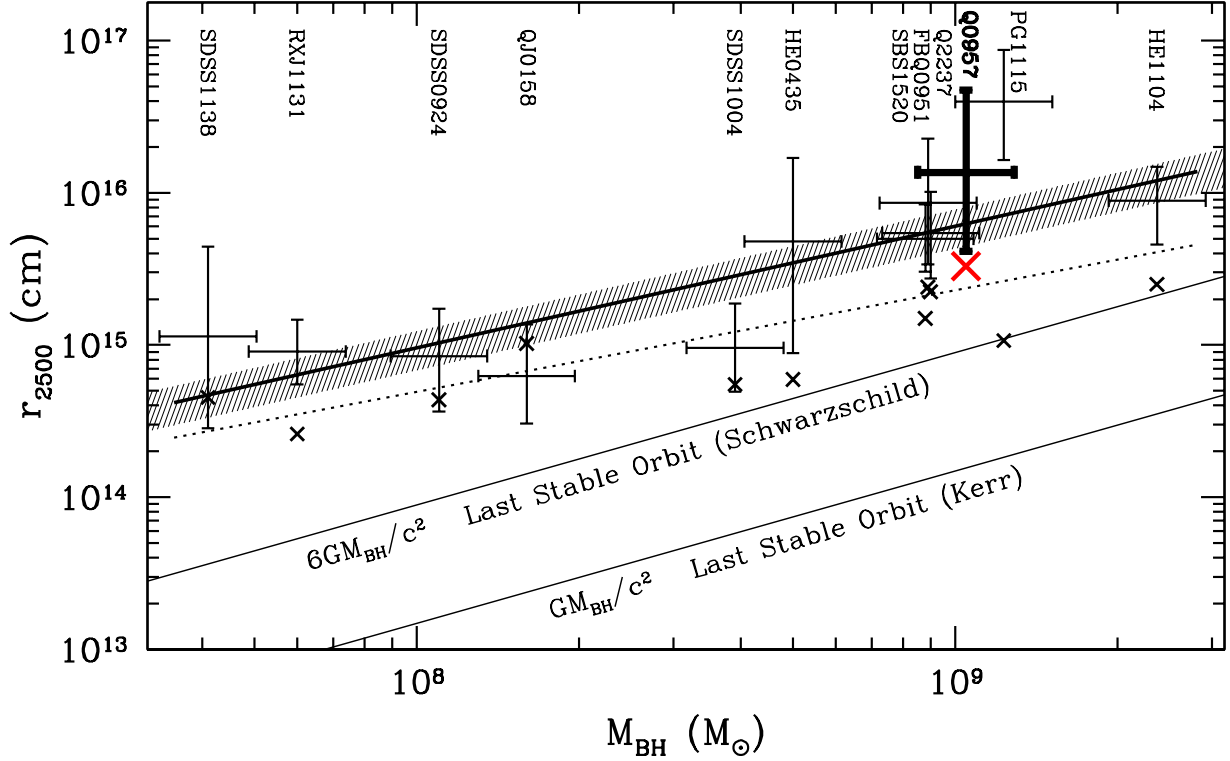


Fig. 6.— Accretion disk size versus supermassive black hole mass relation (thick solid line) and data from Morgan et al. (2010) including the new measurement of r_s for Q0957, scaled to 2500 Å and corrected to 60° inclination. Q0957 is consistent with the mean trend. The dotted line shows the scale radius as a function of central black hole mass predicted by theoretical thin disk models (for $L/L_E = 1/3$ and $\eta = 0.1$), while the diagonal crosses indicate the thin disk size predicted by the magnification-corrected luminosity of the different quasars. We find that Q0957 is consistent with the findings of Morgan et al. (2010) and Blackburne et al. (2011) that the optical continuum sizes of quasars measured through microlensing analyses are larger than the sizes predicted by thin disk theory for a given black hole mass. The microlensing source size for Q0957 is also larger than the luminosity-constrained thin disk size, similar to the findings of Pooley et al. (2007), Morgan et al. (2010) and Mediavilla et al. (2011).